


# Metrological large range magnetic force microscopy

Cite as: Rev. Sci. Instrum. **89**, 093703 (2018); <https://doi.org/10.1063/1.5035175>

Submitted: 13 April 2018 . Accepted: 20 August 2018 . Published Online: 06 September 2018

Gaoliang Dai , Xiukun Hu, Sibylle Sievers, Alexander Fernández Scarioni, Volker Neu , Jens Fluegge, and Hans Werner Schumacher



View Online



Export Citation



CrossMark

## ARTICLES YOU MAY BE INTERESTED IN

[Frontiers of magnetic force microscopy](#)



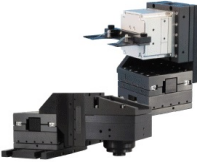
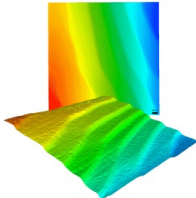
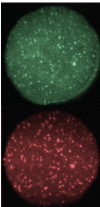
Journal of Applied Physics **125**, 060901 (2019); <https://doi.org/10.1063/1.5050712>

[Direct writing of room temperature and zero field skyrmion lattices by a scanning local magnetic field](#)

Applied Physics Letters **112**, 132405 (2018); <https://doi.org/10.1063/1.5021172>

[Static and dynamic calibration of torsional spring constants of cantilevers](#)

Review of Scientific Instruments **89**, 093701 (2018); <https://doi.org/10.1063/1.5045679>

 <b>MCL</b> MAD CITY LABS INC. <a href="http://www.madcitylabs.com">www.madcitylabs.com</a>	<p>Nanopositioning Systems</p> 	<p>Modular Motion Control</p> 	<p>AFM and NSOM Instruments</p> 	<p>Single Molecule Microscopes</p> 
---	--	--	---	--

## Metrological large range magnetic force microscopy

Gaoliang Dai,<sup>1,a)</sup> Xiukun Hu,<sup>1</sup> Sibylle Sievers,<sup>1</sup> Alexander Fernández Scarioni,<sup>1</sup> Volker Neu,<sup>2</sup> Jens Fluegge,<sup>1</sup> and Hans Werner Schumacher<sup>1</sup>

<sup>1</sup>Physikalisch-Technische Bundesanstalt (PTB), 38116 Braunschweig, Germany

<sup>2</sup>IFW Dresden, Helmholtzstrasse 20, 01069 Dresden, Germany

(Received 13 April 2018; accepted 20 August 2018; published online 6 September 2018)

A new metrological large range magnetic force microscope (Met. LR-MFM) has been developed. In its design, the scanner motion is measured by using three laser interferometers along the x, y, and z axes. Thus, the scanner position and the lift height of the MFM can be accurately and traceably determined with subnanometer accuracy, allowing accurate and traceable MFM measurements. The Met. LR-MFM has a measurement range of 25 mm × 25 mm × 5 mm, larger than conventional MFMs by almost three orders of magnitude. It is capable of measuring samples from the nanoscale to the macroscale, and thus, it has the potential to bridge different magnetic field measurement tools having different spatially resolved scales. Three different measurement strategies referred to as Topo&MFM, MFMXY, and MFMZ have been developed. The Topo&MFM is designed for measuring topography and MFM phase images, similar to conventional MFMs. The MFMXY differs from the Topo&MFM as it does not measure the topography profile of surfaces at the second and successive lines, thus reducing tip wear and saving measurement time. The MFMZ allows the imaging of the stray field in the xz- or yz-planes. A number of measurement examples on a multilayered thin film reference sample made of [Co(0.4 nm)/Pt(0.9 nm)]<sub>100</sub> and on a patterned magnetic multilayer [Co(0.4 nm)/Pt(0.9 nm)]<sub>10</sub> with stripes with a 9.9 μm line width and 20 μm periodicity are demonstrated, indicating excellent measurement performance. © 2018 Author(s). All article content, except where otherwise noted, is licensed under a Creative Commons Attribution (CC BY) license (<http://creativecommons.org/licenses/by/4.0/>). <https://doi.org/10.1063/1.5035175>

### I. INTRODUCTION

To satisfy versatile industrial needs, magnetic stray field measurements require large measurement volumes in the millimeter range in combination with a high spatial resolution on the micro- or nanoscale. This challenging demand holds, for instance, for magnetic sensors, magnetic linear encoders, hard disk data storage, and magnetic random access memory (MRAM) devices. Today, on macroscopic scales, magnetic field measurements are traceable to the international system of units (SI) based on nuclear magnetic resonance (NMR), and traceable calibration chains to the end users are well established.<sup>1</sup> However, such calibration chains to the primary standards are still missing on the micro- and nanoscale.

Magnetic force microscopy (MFM)<sup>2,3</sup> is a widely applied tool for imaging magnetic stray fields.<sup>4</sup> The instrument typically applies a tiny ferromagnetic tip attached to a flexible cantilever which scans close to a specimen surface. During the scan, the dynamic property of the cantilever—typically the phase signal of cantilever's oscillation—is measured, which represents the stray field gradient. In practice, to separate the magnetic interaction between the tip and the sample from other kinds of interactions (e.g., the van der Waals forces), the tip is usually scanned with a lift height of typically tens to hundreds of nanometers above the sample surface. The MFM technique has a high spatial resolution down to 10 nm or even below,<sup>5,6</sup> an important part of the atomic force

microscopy (AFM) technique, which is widely applied for versatile nano-characterisations.

Today, the MFM phase shift images cannot however be easily interpreted quantitatively in terms of local magnetic field data and measurements lack accuracy. This is mainly due to two reasons. The first one relates to the limited accuracy of the scanner motion of MFMs. MFM measurements are sensitive to the tip position with respect to the sample, in particular along the z-axis, due to the rapidly decaying magnetic field, in particular, above nanostructures. To achieve accurate and traceable MFM measurements, the scanner motion must be measured accurately and traceably. Unfortunately, earlier types of MFMs usually use, for instance, a kind of tube scanner, where the scanner position is typically determined from the voltages applied to the piezo scanner. Due to such well-known artifacts as nonlinearity, hysteresis, and creep of piezo materials, the scanner position cannot be measured accurately. Furthermore, the tube scanner movement typically produces a paraboloidal trajectory and causes a bow distortion. To overcome these disadvantages, increasingly more advanced AFMs today apply parallel-kinematics flexure hinge stages as scanners which offer improved orthogonality and minimum out-of-plane motion.<sup>7</sup> To eliminate the influence of limiting properties of piezos, the motion of the scanner is often measured and servo controlled by applying nanometric positioning sensors, such as capacitive sensors, strain gauges, or linear variable differential transducers (LVDTs). Such AFMs offer much better measurement linearity and stability than earlier AFMs and are widely applied in industry today. However, to

<sup>a)</sup> Author to whom correspondence should be addressed: Gaoliang.dai@ptb.de

achieve accurate and traceable results, the positioning sensors of these AFMs must be calibrated regularly, typically by applying a set of nanoscale standards. In turn, these standards must be calibrated prior to their usage, usually by metrological AFMs.<sup>8</sup> In addition to the dimensional property of the scanner, the oscillation amplitude of the MFM tip also needs to be determined to accurately interpret the MFM results. This is usually performed by measuring a tip sample interaction curve (the tip oscillation amplitude vs. the tip sample distance) when a tip interacts with a hard surface such as silicon.

The second reason for measurement inaccuracy with MFMs relates to the challenge in correctly interpreting MFM data. The MFM data resembles the forces or the force gradients of the magnetostatic interaction between the tip's moment and the stray field of the sample. The image is the reflection of the domain structure but not the domain structure itself. It is necessary to apply image processing techniques to obtain reliable domain structure information from MFM images.<sup>9</sup> To solve this challenge, the MFM signal can either be analyzed based on simplified tip-sample interaction models<sup>10,11</sup> or the MFM system can be calibrated by a tip transfer function approach, preferably in Fourier space.<sup>9,12,13</sup>

Furthermore, conventional MFMs available so far only have a limited measurement range, typically of tens of micrometers. This fact limits the measurement capability of MFMs to large-scale samples. The link between magnetic field measurements of different spatially resolved scales (i.e., nano-, micro-, and macroscale) is still missing today.

Recently, in the frame of the European Metrology Programme for Innovation and Research (EMPIR), a project entitled "Nanoscale traceable magnetic field measurements" was set up. The main goal of the project is to develop, test, and validate metrology tools and methods, allowing reliable, quantitative, and traceable measurements of spatially resolved magnetic fields over the entire range from the centimeter down to the micrometer and nanometer length scales. To achieve this target, several key research tasks are being carried out, including the development of metrological MFMs, modeling of the tip sample interaction in MFMs as well as the development of calibration artifacts, and the validation of calibration techniques. In this paper, the development of a unique metrological large range MFM (Met. LR-MFM) will be introduced in detail and its measurement performance will be demonstrated.

## II. THE INSTRUMENT DEVELOPED

A schematic diagram of the Met. LR-MFM developed is shown in Fig. 1(a). The instrument works in the so-called scanning sample principle—during MFM measurements, the MFM tip is kept stationary while the sample is moved along the  $x$ ,  $y$ , and  $z$  axes. To achieve a highly accurate and large range scanning capability, we apply a dual-stage system for scanning samples. The dual stage consists of a piezo positioning stage [shown as the piezoelectric transducer (PZT)-stage in the figure] and a high precision mechanical positioning stage referred to as a nanomeasuring machine (NMM). The PZT stage is a commercial 3-axis parallel-kinematics flexure

hinge stage driven by using piezo actuators (Physik Instrument GmbH, type P915k407). It has embedded capacitive sensors for measuring the actual stage motion in three axes with subnanometer resolution within the motion range of  $15\ \mu\text{m} \times 15\ \mu\text{m} \times 8\ \mu\text{m}$  ( $x$ ,  $y$ ,  $z$ ). The NMM has a motion range of  $25\ \text{mm} \times 25\ \text{mm} \times 5\ \text{mm}$  ( $x$ ,  $y$ ,  $z$ ), developed by the Technical University Ilmenau<sup>14</sup> and is now a commercial product of the SIOS company. The measurement principle of the NMM will be detailed later. As shown in the figure, the sample to be measured ( $s$ ) is fixed on the piezo stage and then mounted on the motion platform of the NMM. Therefore, the actual sample motion is the combined motion paths of two stages. The purpose of the dual-stage design is to achieve both a large motion range and a high motion dynamic, as will be detailed later. The MFM function is realized by a purpose-built AFM head. It measures in the so-called optical lever principle, similar to most commercial AFM devices. Either a laser diode or a superluminescent diode (SLD) can be applied as the light source for measurements in the instrument developed. The SLD has the advantage of short coherence lengths. Therefore, it could eliminate the undesired optical interference phenomenon on the QPD (quadrature photodiode). However, as the light of the SLD is infrared, the usage of a visible laser diode light source offers the advantage of more convenient light beam adjustment. A laser diode light source is therefore applied in this study.

To operate the dual-stage design, a real-time servo controller consisting of two control loops is applied. For clarity, we take the topography measurements in the intermittent-contact AFM mode as an example. The first loop is a fast servo control loop which aims to keep the oscillation amplitude of the AFM bending signal constant. This loop is realized by applying a digital proportional-integral-derivative (PID) controller on the input single  $V_{\text{amp}}$ . The output of the controller is converted from digital to analog, high voltage amplified, and then applied to the  $z$ -piezo actuators of the PZT stage. The PZT stage moves the sample up and down, thus changing the tip sample interaction distance and consequently controlling the AFM value toward the set AFM target value ( $S_1$ ).

The first servo loop keeps the AFM oscillation constant; however, its servo range is limited to the  $z$ -motion range of the PZT stage. To extend this measurement range, another servo loop is applied. In this servo loop, the capacitive signal from the PZT stage is first processed by a capacitive sensor signal processing (CSSP) unit, which outputs a signal  $V_{z\text{cap}}$  representing the  $z$ -extension of the PZT stage. After being analog to digital converted, the  $z$ -extension of the PZT stage is calculated ( $S_{z\text{cap}}$ ) in nanometers. It is then compared to a pre-defined home position ( $S_2$ ) of the PZT stage and finally generates a control target signal  $V_z$ , which commands the NMM to move the sample (together with the PZT stage) up and down. With this servo loop, the extension of the PZT stage is servo controlled toward its predefined home position  $S_2$ .

The two servo loops run simultaneously in a digital signal processor (DSP). As the mechanical dynamic properties of the PZT stage (bandwidth of approximately 300 Hz) are much higher than those of the NMM (bandwidth below 100 Hz), the first servo loop is for following the tip to the surface

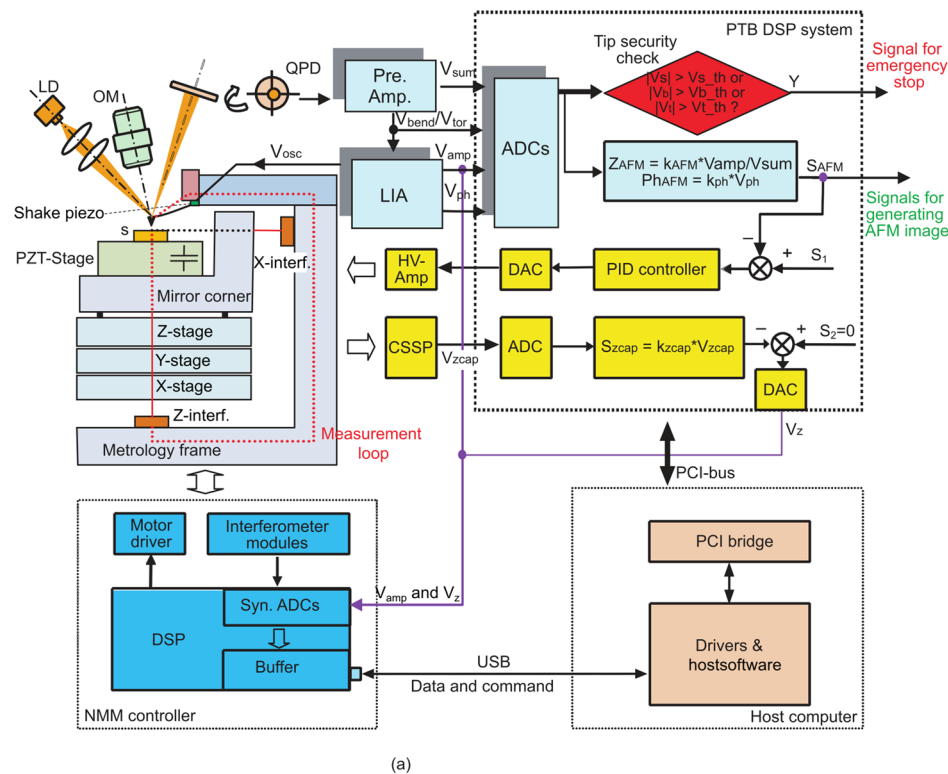
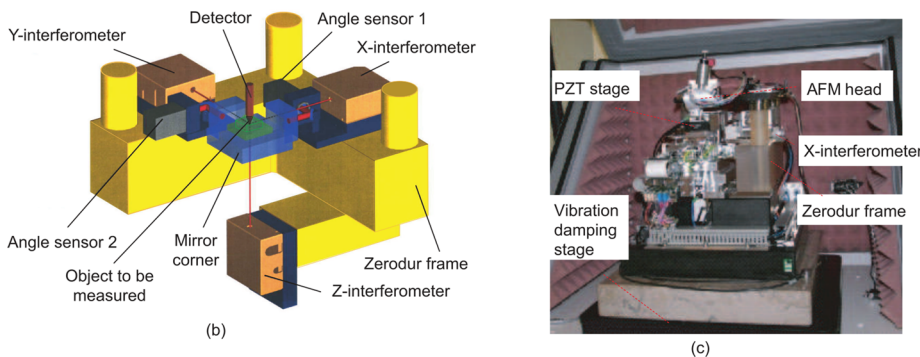


FIG. 1. (a) Schematic diagram of the Met. LR-MFM; (b) schematic diagram of the nanomeasuring machine; and (c) photo of the instrument developed.



topography having higher spatial frequency components (i.e., sharp structure edges and roughness). By contrast, the second servo loop is for following the tip to the surface topography with relatively lower spatial frequency components (i.e., form and waviness). By combining two servo loops (together with the dual-stage design), the AFM can consequently perform AFM scanning both in a large range up to 25 mm × 25 mm × 5 mm (x, y, z) and at high scanning speed up to 1 mm/s.<sup>15</sup> It is to be mentioned that such a large area AFM measurement can be performed directly without the need of stitching multiple small area AFM images.

The metrological principle of the NMM is shown in detail in Fig. 1(b). The motion platform of the NMM consists of a mirror corner which comprises three high-precision planar mirrors attached orthogonally to each other. With three high-precision interferometers (x-, y-, and z-interferometers), the displacement of the motion platform can be measured with respect to the metrology frame (Zerodur frame) with a resolution of 0.08 nm. In addition, there are two angle sensors

available for measuring all three angular degrees of freedom (DOFs) of the motion platform with a resolution of better than 0.01". Thus, all six DOFs of the motion platform are accurately measured in NMM. The motion platform is moved by three stacked mechanical stages driven by voice coil actuators (not shown). By utilizing a DSP servo controller based on the measured 6 DOF values, the NMM is capable of positioning and measuring with nanometer accuracy.

It is to be mentioned that after the sample has approached the MFM tip for measurement, the tip is typically located at the intersection point of three measurement beams of laser interferometers. Thus, the measurement is performed fully in compliance with the Abbe principle along all three axes. The Abbe principle suggests that the displacement of the workpiece in dimensional metrology should be measured coaxially along with the measurement axis of the sensors. It is regarded as a fundamental measurement principle for high accuracy dimensional metrology.



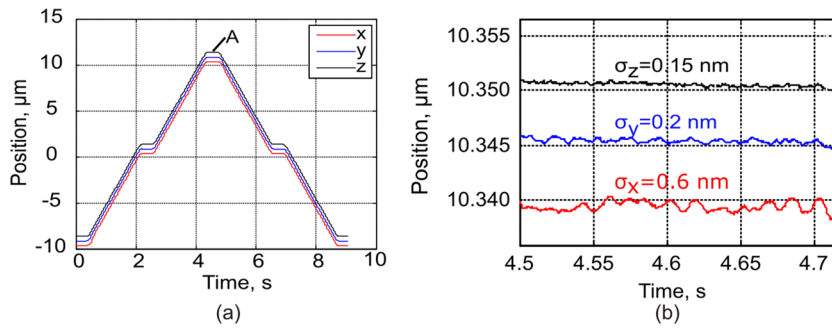


FIG. 2. (a) Measured position of the NMM along the x, y, and z axes when it is commanded to move along three axes simultaneously with a step of  $10\ \mu\text{m}$  and (b) the positioning noise of the NMM after reaching the target position A along three axes.

In the NMM, the interferometers and angular sensors are fixed to a stable metrology frame made of Zerodur which has an ultra-low thermal expansion coefficient. In addition, in the mechanical design, the motion stages and the metrology frame are separately mounted on the instrument base (not shown). This is done in such a way that the variation of the load (due to the weight of the motion stages, the piezo stage, and the sample) during the stage motion will not affect the metrology frame, ensuring high measurement stability.

A photo of the instrument developed is shown in Fig. 1(c). The instrument sits on a passive vibration damping stage and is shielded by an instrument chamber to reduce the influence of acoustic noise as well as to improve temperature stability. The whole instrument is located in the clean room center of Physikalisch-Technische Bundesanstalt (PTB), which has a room temperature stability of  $20 \pm 0.1\ ^\circ\text{C}$ , a humidity of  $46\% \pm 2\%$ , and a clean room class of 1000. No magnetic shielding chamber is used, as the measurement indicates that the influence of environmental magnetic fields on the measurement is not an issue.

To demonstrate the positioning and scanning performance of the instrument, a measurement example is shown in Fig. 2(a), where the NMM is commanded to move along the x, y, and z axes simultaneously by several steps of  $10\ \mu\text{m}$  with a speed of  $5\ \mu\text{m/s}$ . The position noise after arriving at the target positions marked as “A” is shown in Fig. 2(b). It can be seen that the standard deviation of the positioning noise reaches  $0.6\ \text{nm}$ ,  $0.2\ \text{nm}$ , and  $0.15\ \text{nm}$  along the x, y, and z axes, respectively, indicating the excellent positioning performance of the instrument.

### III. MEASUREMENT EXAMPLES

Three different MFM measurement strategies have been realized in the Met. LR-MFM developed, as shown in Fig. 3. As the sample may be misaligned when it is mounted on the instrument, its tilting angles in the xz- and yz-planes are usually determined *prior to* the MFM measurements, e.g., by measuring two topographic profiles along the x- and y-directions. Such tilting angles are then fully compensated for in the MFM measurements. The first measurement strategy is referred to as Topo&MFM. It functions in a similar way to most commercial MFMs. As shown in Fig. 3(a), the measurement in the Topo&MFM consists of four steps. First, the topography of the sample is measured in the intermittent-contact mode. Then, the tip is lifted to a defined height ( $H_0$ ). As the third step, the tip scans over the sample at the lifted height, and the phase signal is recorded as the MFM signal. And finally, the tip lands on the sample surface again for the measurement of the next lines. Furthermore, owing to the highly precise positioning stage, the Met. LR-MFM is capable of measuring topography in the trace scan and the MFM signal in the retrace scan. It can thus reduce the measurement time by a factor of 2 compared to commercial MFMs.

The second strategy is referred to as MFMXY, as shown in Fig. 3(b). Using this strategy, the first line is measured in a similar way to that of the Topo&MFM, where a topography profile is first scanned and then an MFM profile is measured at a lift height of  $H_0$ . However, different to the Topo&MFM, it does not measure the topography profile for the successive profiles. Instead it uses the surface slopes measured in the first

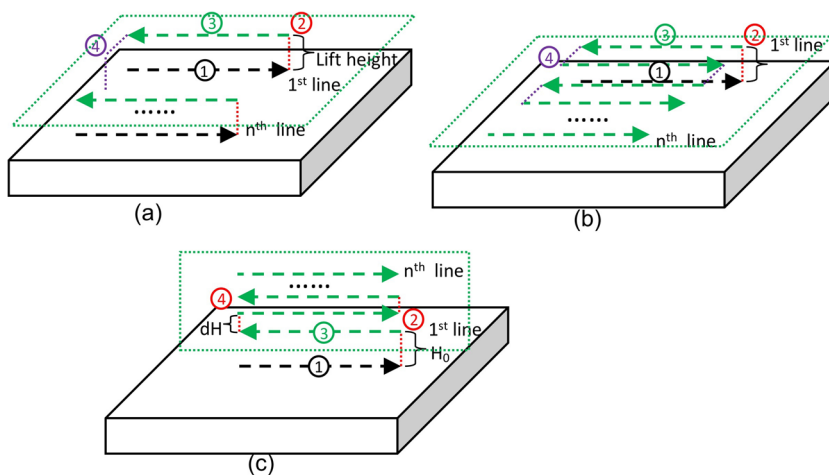


FIG. 3. Schematic diagram of three different MFM measurement strategies, shown as (a) Topo&MFM, (b) MFMXY, and (c) MFMZ.

topography profile for calculating the tip path, as a straight line, parallel to the surface, for MFM measurements. This strategy has the advantage of much less tip wear, as there is almost no tip wear in the lifted MFM measurements. In addition, it reduces the measurement time by an additional factor of 2. However, an issue that needs to be dealt with is the instrument drift, particularly in the z-axis, as it may change the lift height, thus leading to significant measurement errors. To solve this problem, a drift compensation mechanism is designed. It determines the actual z-position of the surface by landing the tip on the surface at a predefined time interval. No topography scan is needed in this drift compensation process; therefore, it can be carried out within a short time ( $<5$  s) and without the risk of tip wear. With this drift compensation mechanism, the lift height can be kept with an accuracy better than 1 nm throughout the MFM measurement.

When using the MFMXY strategy, there is, in addition, a software option to disable the measurement of the first topography profile. It is designed for two measurement scenarios—(i) super-sharp MFM tips and (ii) “uncooperative surfaces.” Super-sharp MFM tips offer advantages of super-fine spatial measurement resolution. However, there is a high risk of such a sharp tip being worn down even in the first line topography scan. Disabling the topography profile scan is therefore an ultimate solution for avoiding tip wear. “Uncooperative surfaces” are surfaces whose topography cannot be measured by AFM tips, such as surfaces with features having a height over tens of micrometers.

Topo&MFM and MFMXY, the measurement strategies just introduced, are designed for measuring the magnetic stray field in an xy-plane with a given lift height. To enable the measurements in an xz- or a yz-plane, a third measurement strategy, referred to as MFMZ, has been designed as shown in Fig. 3(c). Its measurement procedure is similar to that of MFMXY. The difference is that it changes the lift height by a predefined step,  $dH$ , in the successive lines. The drift compensation mechanism is also implemented in this strategy.

A number of measurements have been performed on a magnetic reference sample using the instrument developed. The sample is a multilayered thin film made of  $[\text{Co}(0.4 \text{ nm})/\text{Pt}(0.9 \text{ nm})]_{100}$ , which possesses a perpendicular magnetic anisotropy.<sup>13</sup> In the as-prepared, demagnetized state, it develops a maze domain structure with an average domain width of approximately 170 nm.

Figure 4 shows the measurement of the sample using the Topo&MFM strategy. The sample is measured in an area with a size of  $5 \mu\text{m} \times 5 \mu\text{m}$  by  $512 \times 512$  pixels. The scanning speed for the topography and MFM measurements is  $10 \mu\text{m/s}$ . An MFM probe type PPP-MFMR from nanosensors has been applied for the measurement. It has a resonance frequency of 78.2 kHz and a quality factor  $Q$  of 220, as determined by the automatic tip frequency tuning function of the Met. LR-MFM. For MFM measurements, the free tip oscillation amplitude is set as 17 nm and the lift height  $H_0$  is set as 50 nm. The measured topography image is plotted in Fig. 4(a) together with a cross-sectional profile at the marked position [Fig. 4(c)]. The image is shown as the raw data after a first order linear fit, which is typically applied to correct the inclination of the sample surface introduced by a sample mounting error. The topography image shows that the sample surface topography is rather smooth. The grain structure of the thin film has a typical height of 1-2 nm, although some taller structures exist which may be attributed to contamination. It can be seen that the measured topography image is very flat and no parabola is visible. This is due to the outstanding metrological performance of the instrument. The measured MFM phase image is plotted in Fig. 4(b), and a cross-sectional profile at the marked position is illustrated in Fig. 4(d), shown as the raw measurement data without any filtering. It has a good contrast and resolves the nanoscale magnetic domain structure very well.

Figure 5 illustrates a measurement example performed using the MFMXY strategy. The sample is measured in an area with a size of  $5.0 \mu\text{m} \times 5.0 \mu\text{m}$  and  $512 \times 512$  pixels and with

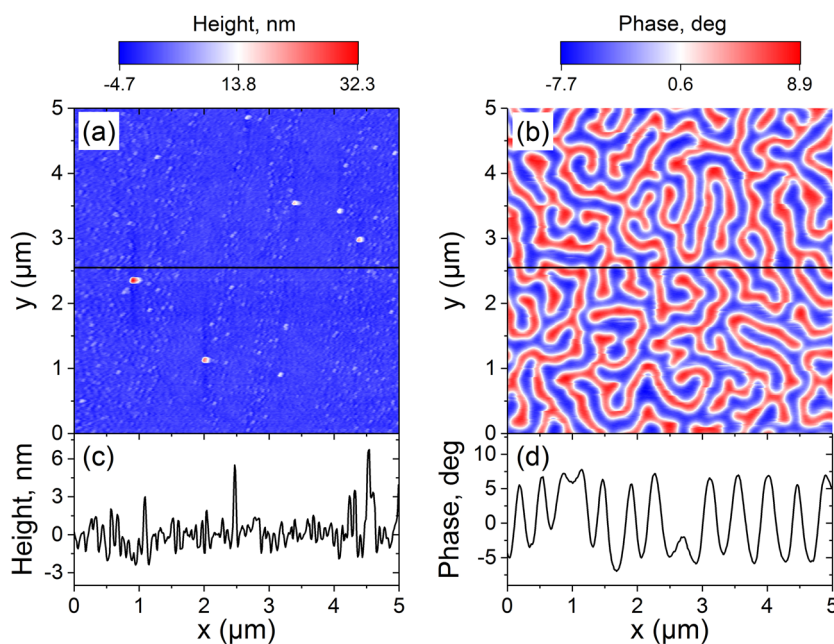


FIG. 4. Measured result of the Met. LR-MFM when it is operated in the Topo&MFM mode, shown as (a) the topography AFM image and (b) the MFM phase image. Cross-sectional profiles of the topography and phase image at the marked position are shown in (c) and (d), respectively.

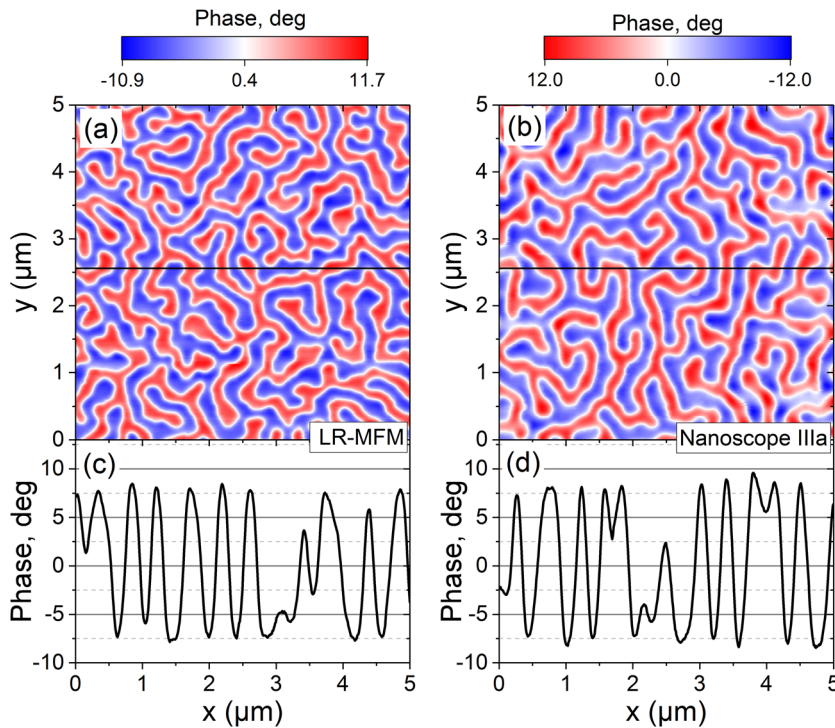


FIG. 5. Measured result of the Met. LR-MFM when it is operated in the lifted MFMXY mode, shown as (a) the MFM phase image and (c) cross-sectional profiles at the marked position shown in (a). For comparison, the sample is measured by a commercial MFM instrument (type Nanoscope IIIa) using the same MFM tip with similar measurement parameters, shown as (b) the MFM phase image and (d) cross-sectional profiles at the marked position shown in (b).

a scanning speed of  $10 \mu\text{m/s}$ . The free tip oscillation amplitude is changed to  $14.4 \text{ nm}$  and the lift height to  $45 \text{ nm}$ . The drift compensation mechanism is used in this measurement, which brings the tip to the surface every four lines. The measured MFM phase image is plotted in Fig. 5(a), and a cross-sectional profile at the marked position is shown in Fig. 5(c) as the raw data. It can be seen that the obtained MFM image has a similar quality to that of the Topo&MFM, confirming the feasibility of the MFMXY measurement strategy. As the MFMXY strategy has the advantage of less tip wear and shorter measurement times, we currently use the MFMXY strategy more frequently than the Topo&MFM. Figures 5(b) and 5(d) depict an MFM phase image measured on the same sample by a commercial MFM instrument (type Nanoscope IIIa) using the same MFM tip. The measurement conditions are supposed to be the same in this comparison. There are however slight differences in practice. For instance, the quality factor of the MFM tip is measured to be 220 in the Met. LR-MFM, while it is 218 in the Nanoscope IIIa. This is attributed to the different cantilever clamping mechanics of the two instruments leading to different energy losses. Furthermore, the free tip oscillation amplitude and the lift height of the Nanoscope IIIa cannot be determined precisely because of the lack of traceable displacement measuring sensors. Although a direct and quantitative comparison of the two instruments is thus infeasible, the MFM images presented here show rather similar quality. However, compared to commercial MFM instruments, the Met. LR-MFM has advantages in traceably and precisely measuring the lift height and the tip oscillation amplitude needed for the accurate determination of the magnetic stray field.

High measurement stability and repeatability are generally prerequisites for achieving high measurement accuracy for a metrological instrument. To investigate the measurement

stability of the Met. LR-MFM developed, several MFM measurements are performed with the fast scan axis disabled. In such a way, the same profile is scanned repeatedly in the measurement. A typical MFM phase image is shown in Fig. 6(a), and two cross-sectional profiles at the 50th and 60th lines of the image are plotted in Fig. 6(b), shown as the raw data. The two profiles overlap very well. A very slight difference ( $<0.1^\circ$ ), as shown in a zoomed-in view, indicates very high measurement stability and repeatability. The standard deviation over 512 phase profiles is evaluated as  $0.13^\circ$ , which is better than that of the Nanoscope IIIa ( $0.19^\circ$ ) determined in the same way. As electronic and mechanical noise as well as the environmental magnetic stray field may disturb the measurement results, this result confirms not only the low noise of the instrument but also the small influence of the environmental magnetic stray field. It is important to confirm this issue because the NMM applies voice coils as motion actuators. Principally, such voice coils may have some stray magnetic field leakage, thus impacting the measurement results. However, such an influence is small owing to two factors: the small current applied to the voice coils and the large spatial distance from the voice coils to the sample.

Figure 7 illustrates a measurement example using the MFMZ strategy. The sample is measured with a profile length of  $5 \mu\text{m}$  and 512 pixels in a scanning speed of  $10 \mu\text{m/s}$  along the y-axis. The lift height is initially  $50 \text{ nm}$  and is increased to  $300 \text{ nm}$  in steps of  $2 \text{ nm}$ . An MFM phase image is shown in Fig. 7(a), which represents the magnetic stray field in the yz-plane with a size of  $5.11 \mu\text{m} \times 250 \text{ nm}$ . Three phase profiles at a lift height of  $50 \text{ nm}$ ,  $80 \text{ nm}$ , and  $130 \text{ nm}$ , respectively, are plotted in Fig. 7(b). It can be seen that the strength of the magnetic stray field decreases rapidly with respect to the increased lift height.



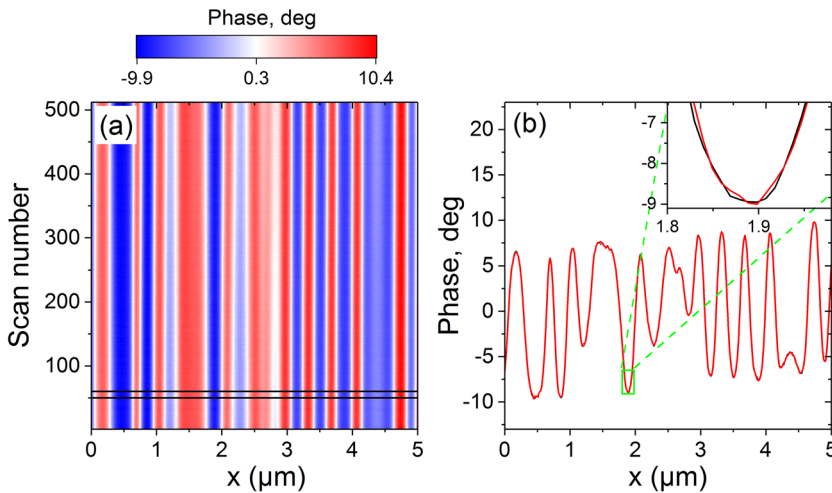


FIG. 6. To check the measurement repeatability, an MFM phase image is recorded when its slow scan axis is disabled, as shown in (a). Two cross-sectional profiles at the 50th and 60th lines are plotted in (b). Due to the high measurement stability, the two profiles overlap very well in (b). However, slight differences can be observed in an inset figure which gives a zoomed-in view of the phase profile at the marked area.

To investigate the relationship between the strength of the phase signal and the lift height, we calculate the strength of the phase signal in a profile as its root mean square (RMS) value as

$$Ph_q = \sqrt{\frac{\sum_{i=1}^N (Ph_i - \bar{Ph})^2}{N}}, \quad (1)$$

where  $Ph_i$  is the measured phase value of the  $i$ -th pixel of the profile and  $\bar{Ph}$  is the arithmetical mean of the phase values of the profile.  $N$  is the number of pixels of the profile.

The relationship between  $Ph_q$  and lift height,  $H$ , is plotted in Fig. 7(c).  $Ph_q$  shows a quasi-exponential decay with respect to  $H$ , agreeing well with the theoretical analysis.<sup>12</sup> In fact, the analysis in Ref. 12 shows that it cannot be strictly exponential since different spatial Fourier components decay with different wave length-dependent decay exponents. Thus, a more critical analysis should consider the decay behavior of magnetostatic quantities in its mathematically exact formulation. For the MFM signal,  $MFM(x, y, z_0)$  (e.g., phase shift) at a given plane above the flat sample surface (distance  $z_0$ ) and the signal at a higher distance  $z = z_0 + \Delta z$ , the following relation holds:<sup>12</sup>

$$\overline{MFM}(\vec{k}, z_0 + \Delta z) = \overline{MFM}(\vec{k}, z_0) e^{-k\Delta z}. \quad (2)$$

Here,  $\vec{k} = (k_x, k_y)$  is the two-dimensional wave vector,  $\overline{MFM}(\vec{k})$  is the Fourier transform of the MFM signal, and  $k = \sqrt{k_x^2 + k_y^2}$ . Based on this equation,  $Ph_q$  values for the same line at different lift heights are calculated from Fig. 5(a) with  $z_0 = 50$  nm, shown as a red line in Fig. 7(c). The experimental result is in excellent agreement with the theoretical calculation.

To demonstrate the large range measurement capability of the Met. LR-MFM developed, measurements are performed on a patterned sample consisting of magnetic stripes with a width of 9.9  $\mu\text{m}$ , a pitch of 20  $\mu\text{m}$ , and a height of 50 nm. The sample is fabricated from a magnetic multilayer of Ta(20 nm)/Pt(5 nm)/[Pt(0.9 nm)/Co(0.4 nm)]<sub>10</sub>/Pt(2 nm) with strong out-of-plane magnetic anisotropy sputter deposited on top of a Si substrate covered with SiO<sub>2</sub> provided by the Leibniz Institute for Solid State and Materials Research Dresden (IFW). The micrometer-scale stripe structures were patterned using electron beam lithography in combination with argon etching. Their magnetic features thus consist of a periodic arrangement of magnetic and non-magnetic areas (stripes) on the 10  $\mu\text{m}$  scale. Within the magnetic areas, both micrometer-sized single domains and submicrometer-sized fine patchy domains are seen. These types of domains are typical for magnetic films with perpendicular anisotropy and a film thickness

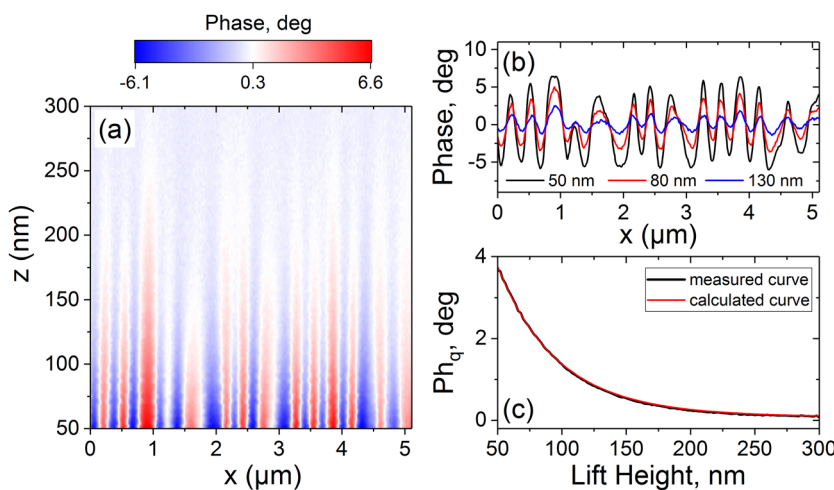


FIG. 7. (a) An MFM phase image measured in the MFMZ mode when the lift height  $H$  is changed from 50 nm to 300 nm; (b) cross-sectional phase profiles measured at the lift height of 50 nm, 80 nm, and 130 nm, respectively; (c) the relationships between the measured phase signal strength (black) and calculated signal strength (red) based on Eq. (2) vs. the lift height.



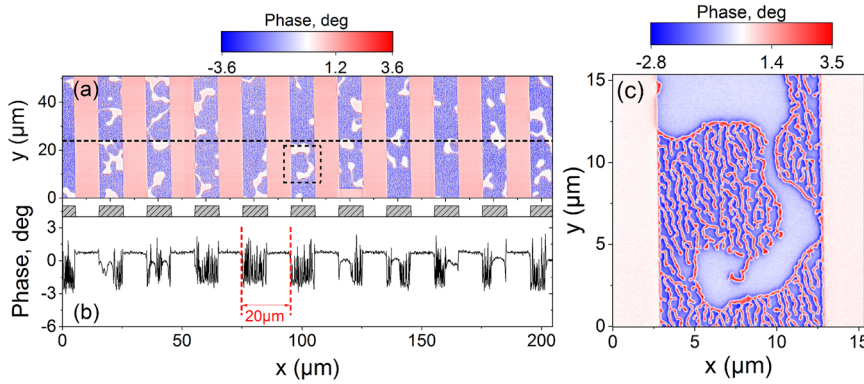


FIG. 8. Demonstration of a large range MFM measurement, shown as (a) an MFM phase image measured on a patterned magnetic multilayer sample over an area of  $204.7 \mu\text{m} \times 51.1 \mu\text{m}$  ( $x, y$ ); (b) a cross-sectional profile at the marked line in (a); and (c) a zoomed-in MFM phase image measured over an area of  $15.33 \mu\text{m} \times 15.33 \mu\text{m}$  marked as the dashed square in (a).

below the critical thickness of  $l_c = \gamma/2K_d$  ( $\gamma = 4\sqrt{A \cdot K_u}$ ,  $K_d = 0.5\mu_0 M_s^2$ ,  $A$  = exchange constant,  $K_u$  = perpendicular anisotropy, and  $M_s$  = saturation magnetization), as is the case for this 13 nm thin multilayer, as opposed to the 130 nm thick sample studied above. The sample is measured using the MFMXY strategy and with a lift height of 50 nm. A large area of  $204.7 \mu\text{m} \times 51.1 \mu\text{m}$  is measured directly by  $2048 \times 512$  pixels at a scanning speed of  $10 \mu\text{m/s}$  without image stitching. A measured MFM phase image is shown in Fig. 8(a) as the raw data, and a cross-sectional profile at the marked line is depicted in Fig. 8(b). The micrometer-sized domain structure is clearly visible in Fig. 8(a), agreeing well with the material property. Such large and coarse overview scans are intended for reducing the measurement time. However, the sub- $\mu\text{m}$ -sized patchy domains are not well resolved due to the large pixel size selected. Thus, to resolve the fine domains, a region of interest (ROI) with a size of  $15.33 \times 15.33 \mu\text{m}^2$  has been selected and measured with a higher resolution of  $512 \times 512$  pixels, as demonstrated in Fig. 8(c). The large-area measurement capability and the zoom-in function together with the high measurement accuracy of the instrument offer unique performances of the developed tool.

#### IV. CONCLUSION

Magnetic force microscopy (MFM) has been widely applied for measuring nanoscale magnetic stray fields with a spatial resolution down to 10 nm or even below. Today MFM measurements are however usually qualitative and lack accuracy due to insufficient dimensional measurement accuracy as well as the challenge in interpreting the MFM data. In addition, conventional MFM available so far only has a limited measurement range, typically of tens of micrometers. This limits the measurement capability of MFM to large-scale samples and to linking the quantitative magnetic stray field measurements between nanoscale, microscale, and macroscale.

This paper presents the development of a unique metrological large range MFM (Met. LR-MFM) with a measurement volume up to  $25 \text{ mm} \times 25 \text{ mm} \times 5 \text{ mm}$ . The instrument works in a scanning sample principle. To achieve both a large measurement range and a high measurement speed, a dual-stage design which combines a parallel-kinematics flexure hinge piezo stage and a precision mechanical positioning stage (referred to as a nanomeasuring machine, NMM) has been applied for scanning samples in the  $x, y$ , and  $z$  axes. Owing to

the high precision nanometric laser interferometers and angular sensors applied for measuring all six degrees of freedom of the sample position fully in compliance with the Abbe principle, the sample can be positioned with nm accuracy. The experimental results show the position stability reaches 0.15 nm, 0.2 nm, and 0.6 nm along the  $x, y$ , and  $z$  axes, respectively. The instrument applies a purpose-built AFM head. It applies an optical lever for measuring the bending and torsion of cantilevers. It is capable of measuring in the contact, intermittent, and non-contact AFM modes.

Three different measurement strategies referred to as Topo&MFM, MFMXY, and MFMZ have been realized in the system. The Topo&MFM measures the topography profile of a surface in the intermittent-contact mode first, and then, the tip is lifted for measuring magnetic stray fields in the non-contact mode, similar to conventional MFMs. The MFMXY differs from the Topo&MFM in that it does not measure the topography profile of surfaces at successive lines. It offers advantages in reducing tip wear and saving measurement time. To account for the influence of the instrument drift particularly along the  $z$ -axis, a drift compensation mechanism is implemented in this measurement strategy. The MFMZ measurement strategy makes it possible to image the stray field along the  $xz$ - or the  $yz$ -plane.

A number of selected measurement examples have been demonstrated to illustrate the measurement capability and performance of the developed device. The results indicate the good measurement performance and high measurement stability and repeatability of the device developed.

The Met. LR-FM developed offers an excellent instrument base for traceable and quantitative measurements of magnetic stray fields at the nanoscale. In the near future, more research work will be carried out in interpreting the measured MFM data based on the modeling of the MFM measurement. Furthermore, calibration artifacts and calibration procedures for traceable measurements of magnetic stray fields will be developed.

#### ACKNOWLEDGMENTS

The EMPIR is jointly funded by the EMPIR participating countries within EURAMET and the European Union. We thank the European Commission and the EURAMET e.V. for their financial support within EMRP/EMPIR JRP's 15SIB06 NanoMag.

- <sup>1</sup>K. Weyand, "An NMR marginal oscillator for measuring magnetic fields below 50 mT," *IEEE Trans. Instrum. Meas.* **38**(2), 410–414 (1989).
- <sup>2</sup>J. J. Saenz, N. Garcia, P. Grütter *et al.*, *J. Appl. Phys.* **62**, 4293 (1987).
- <sup>3</sup>Y. Martin and H. K. Wickramasinghe, "Magnetic imaging by 'force microscopy' with 1000 Å resolution," *Appl. Phys. Lett.* **50**, 1455 (1987).
- <sup>4</sup>E. Meyer, H. J. Hug, and R. Bennewitz, *Scanning Probe Microscopy* (Springer-Verlag, Berlin, Heidelberg, 2004).
- <sup>5</sup>A. Moser, M. Xiao, P. Kappenberger *et al.*, "High-resolution magnetic force microscopy study of high-density transitions in perpendicular recording media," *J. Magn. Magn. Mater.* **287**, 298–302 (2005).
- <sup>6</sup>Z. Li, X. Li, D. Dong, D. Liu, H. Saito, and S. Ishio, "AC driven magnetic domain quantification with 5 nm resolution," *Sci. Rep.* **4**, 5594 (2014).
- <sup>7</sup>J. Kwon, J. Hong, and Y. Kim, "Atomic force microscope with improved scan accuracy, scan speed, and optical vision," *Rev. Sci. Instrum.* **74**(10), 4378–4383 (2003).
- <sup>8</sup>G. Dai *et al.*, "A metrological large range atomic force microscope with improved performance," *Rev. Sci. Instrum.* **80**, 043702 (2009).
- <sup>9</sup>D. Wu, Y. Lou, F. Zheng *et al.*, "The Fourier analysis of magnetic force microscopy imaging," *J. Appl. Phys.* **112**, 063913 (2012).
- <sup>10</sup>S. Vock, F. Wolny, T. Mühl *et al.*, *Appl. Phys. Lett.* **97**, 252505 (2010).
- <sup>11</sup>T. Häberle, F. Hering, H. Pfeifer *et al.*, *New J. Phys.* **14**, 043044 (2012).
- <sup>12</sup>H. J. Hug, B. Stiefel, P. J. A. Schendel *et al.*, "Quantitative magnetic force microscopy on perpendicularly magnetized samples," *J. Appl. Phys.* **83**, 5609 (1998).
- <sup>13</sup>S. Vock, C. Hengst, M. Wolf *et al.*, "Magnetic vortex observation in FeCo nanowires by quantitative magnetic force microscopy," *Appl. Phys. Lett.* **105**, 172409 (2014).
- <sup>14</sup>G. Jäger, E. Manske, T. Hausotte, and H. J. Büchner, "Laserinterferometrische Nanomeßmaschinen," in *Sensoren und Messsysteme 2000*, VDI-Berichte 1530 (VDI-Verlag, 2000), pp. 271–278.
- <sup>15</sup>G. Dai, F. Zhu, and J. Fluegge, "High-speed metrological large range AFM," *Meas. Sci. Technol.* **26**, 095402 (2015).